Morphogenetic Metasurface Engineering for Computational Localization Applications

Raymundo Amorim, Yann Marie-Joseph, Cyril Decroze, Thomas Fromenteze

Morphogenetic Metasurface Engineering for Computational Localization Applications

Raymundo Amorim
University of Limoges,
XLIM, UMR 7252,
F-87000 Limoges, France

Cyril Decroze
University of Limoges,
XLIM, UMR 7252,
F-87000 Limoges, France

Thomas Fromenteze
University of Limoges,
XLIM, UMR 7252,
F-87000 Limoges, France

***Abstract*—This paper presents a bio-inspired generative model allowing the emergence of self-organized spatial patterns exploited for the design of frequency-diverse metasurface antennas. The latter radiate patterns that are weakly correlated in space and frequency are adapted to the direction of arrival detection applications operating in a simplified hardware-oriented approach. The generative model studied automates the design of these metasurfaces by ensuring statistical control of certain key properties. To this end, demonstration antennas are evaluated in terms of quality factor and radiation efficiency. In line with previous demonstrations of computational localization techniques, a set of simulations is proposed to study the performance of new classes of frequency-diversity metasurfaces, referred to as morphogenetic.**

***Index Terms*—Metasurface antennas, morphogenetic generation, direction of arrival, computational localization**

I. Introduction

Practical localization systems attempt to optimize the trade-off between reliability and ease of implementation against the system complexity. The optimization of the trade-off between hardware complexity and cost-effectiveness paves the way for new solutions based on direction of arrival (DoA) applications. The simplest DoA architectures are based on mechanical scanning of high-gain antennas, limited by low data acquisition speeds and wear and tear on moving parts. Electronic scanning of antenna arrays is a much faster alternative. However, these techniques require the use of highly redundant active systems associated with each antenna, enabling beamforming in the hardware layer using phase shifters and amplifiers, or in the software layer following the digitization of all received signals.

In contrast to conventional approaches, frequency-diverse metasurface antennas and computational techniques are proposed for relaxing hardware constraints, suggesting a significant potential for enhancing DoA capability [1]. Frequency-diverse metasurface antennas can reduce design complexity while maintaining electromagnetic performance. Additionally, different from conventional approaches, computational techniques do not require additional control systems, shifting constraints to the digital layer. This hardware-oriented approach enables a cost-effective solution while also offering a potentially adapted design to conventional low-cost fabrication methods.

These developments are proposed in recent imaging and localization demonstrations highlighting the contribution of computational techniques to optimizing the trade-off between hardware design, simplicity of data acquisition and reliable electromagnetic performances [1]–[6]. The common objective of these projects is to limit the hardware complexity of active systems by developing antennas radiating series of spatially uncorrelated field distributions, reconfigured in a wide range of demonstrations by means of a simple frequency sweep. These approaches also leverage recent advances in compressive sensing, exploiting the spatial structures of regions of interest to reduce the number of measurements needed for their reconstruction. In [1], [2], demonstrations of computational imaging and angle of arrival detection are proposed using a frequency diversity antenna, implemented with a leaky volumetric cavity. Modal diversity is crucial for these applications as it represents the support of the measured information, justifying the use of 3D components large relative to the operating wavelengths. The latter are thus limited by a reduced integration capacity and relatively high machining costs.

Single-layer antenna designs are reported in [3], [4]. A significant step is noted toward simple designs maintaining modal diversity. Metallic vias were placed on the edges of the metasurfaces introduced in these papers to form two-dimensional cavities, ensuring better field confinement to limit the overlap of resonance modes. However, this approach has the disadvantage of increasing the number of steps required for the fabrication of such antennas. The designs most similar to the metasurfaces generated in our present work are undoubtedly those found in [5], [6], which describe a single-layer antenna fabricated on a printed circuit board. This cavity structure features radiating irises arranged in a Fibonacci pattern. However, despite its overall size, this structure exhibits a limited number of modes.

An essential factor that thoroughly limits the metasurface antenna design is the inherent trade-off between quality factor (Q-factor) and antenna radiation efficiency [2]. High Q-factors reflect the ability to generate uncorrelated radiated field patterns for a given leaky cavity size. However, as the Q-factor increases, the radiation efficiency is reduced due to better field confinement. Consequently, it is notoriously challenging to design frequency-diverse metasurfaces simultaneously optimized in Q-factor and radiation efficiency.

This work presents an automated method based on a bio-inspired generative model for designing frequency-diversity

metasurface [7]. This new approach aims to provide an alternative for advanced control of the electromagnetic characteristics required for the proper operation of computational techniques. This generative model enables the constrained self-structuring of spatial patterns, making it possible to conceive frequency-diverse metasurfaces with controlled Q-factor, radiation efficiency and operating bandwidth for computational DoA applications.

The synthesis of such antennas is inspired by the theory of morphogenesis introduced by Alan Turing [8], leading to the designation of morphogenetic metasurfaces. The generative model considered is detailed in section II. In Section III, simulations are carried out considering different classes of Gray-Scott patterns, enabling electromagnetic performances to be evaluated. Finally, in Section IV, the DoA application is studied.

II. Morphogenetic frequency-diverse metasurface antennas

A proof-of-concept antenna design based on a reaction-diffusion model is investigated. This method focuses on providing a family of frequency-diverse antennas while providing a simplified and automated generation process. First, the Gray-Scott reaction-diffusion model is described.

A. Gray-Scott model

The Gray-Scott model is a simple system of partial differential equations inspired by chemical processes [7]. This reaction-diffusion model involves two species $\mathbf{U}$ and $\mathbf{V}$ which tend to occupy the available space and interact to form spatial patterns when the model is correctly parameterized. The unique generated bio-inspired patterns can be exploited to create metasurface frequency-diverse antennas. The model is defined by Eqs. (1):

$$\frac{\partial \mathbf{U}}{\partial t} = d_u \nabla^2 \mathbf{U} - \mathbf{U}\mathbf{V}^2 + f(1-\mathbf{U}) \tag{1a}$$

$$\frac{\partial \mathbf{V}}{\partial t} = d_v \nabla^2 \mathbf{V} + \mathbf{U}\mathbf{V}^2 - (f+k)\mathbf{V}, \tag{1b}$$

where $\mathbf{U}$ and $\mathbf{V}$ stand for to the morphogen concentrations, d_u and d_v corresponds to diffusion coefficients. The f and k correspond to the feed rate and kill rate, respectively. The reaction-diffusion patterns for different couples of parameters f and k are depicted in Fig. 1. The generation is computed by finite difference with $d_u = 1$, $d_v = d_u/3$ and $dt = 0.875$. Morphogen concentrations are initialized to $\mathbf{U} = 0$ and $\mathbf{V} = 1$, apart from a rectangular subdomain which is randomly perturbed to a concentration of 0.5 to trigger pattern synthesis.

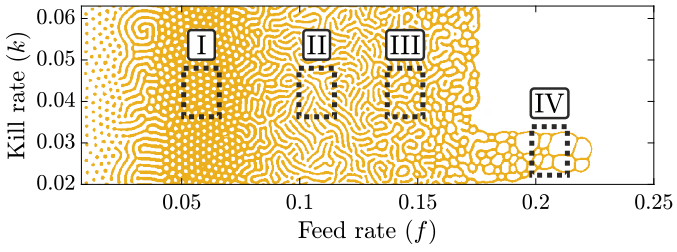

Fig. 1: Self-organized morphogens patterns for a domain 1000×300 pixels. Four classes of patterns are studied, considering the associated (f, k) parameter pairs for metasurface synthesis in the rest of the study.

Four regions are arbitrarily selected to generate the metasurface antenna designs (Fig. 1). This model can create spatial distributions of patterns influencing the statistics of induced currents on the generated metasurfaces. By changing only the initialization of the $\mathbf{U}$ and $\mathbf{V}$ matrices, the pattern types remain constrained, but their spatial distribution will be completely different. This approach thus provides collections of morphogenetic metasurfaces with controlled average characteristics, each realization of which is unique.

B. Evaluation of morphogenetic frequency-diverse metasurface antennas

Based on the generated Gray-Scott patterns, a family of four regions is selected: (I) irises, (II) stripes, (III) irises and stripes, and (IV) dryland. These regions have unique pattern characteristics and their arrangement influences induced surface currents that favor the coupling between cavity modes, which can improve the radiation of uncorrelated far field distributions. The associated antennas are depicted in Fig 2.

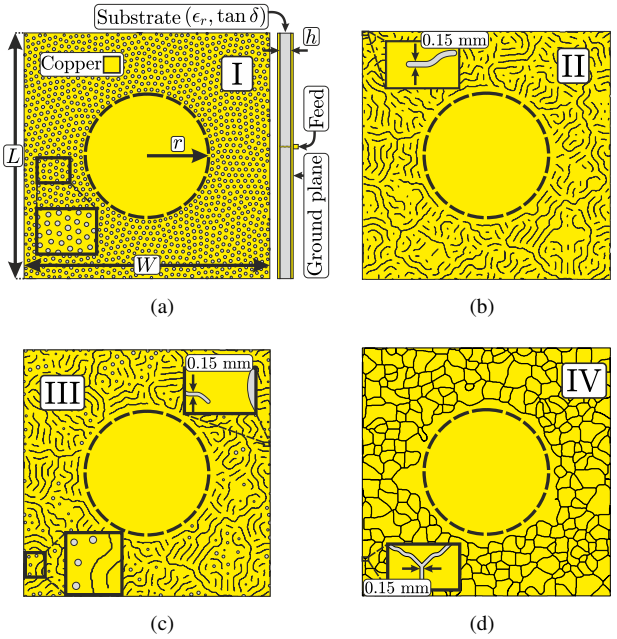

Fig. 2: Metasurface antennas based on the Gray-Scott reaction-diffusion model (a) irises, (b) stripes, (c) irises and stripes and (d) dryland. These antenna designs have 650×650 pixels each.

The antennas are built on the same substrate characteristics; a 150×150 mm^2 Rogers 4003C substrate with relative permittivity $\epsilon_r = 3.55$ and loss tangent $\tan\delta = 0.0027$, and a thickness $h = 0.813$ mm. The metasurfaces are fed by a coaxial connector passing through the substrate and welded to

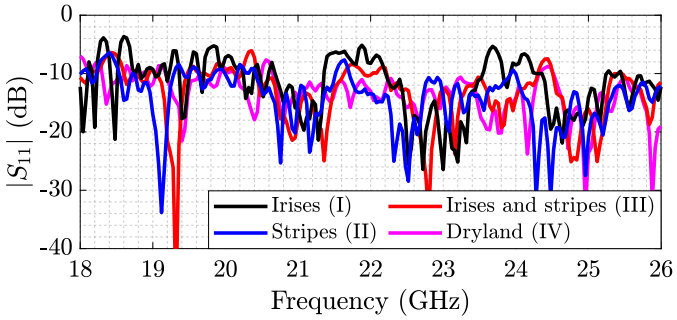

Fig. 3: Magnitude of the reflection coefficients $|S_{11}|$.

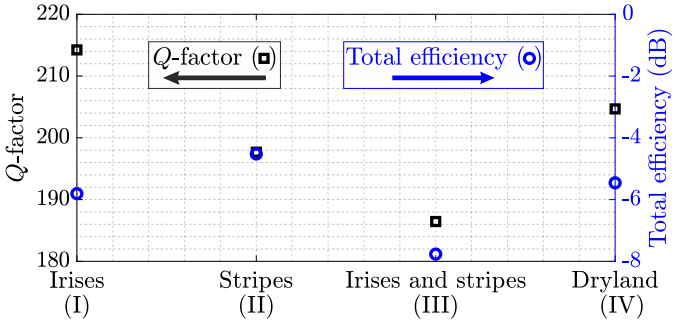

Fig. 4: Q-factor and total radiation efficiency of the proposed antennas.

the upper conductor, formed by a disk of radius $r = 40$ mm where the growth of morphogens is prohibited.

For each type of pattern, the following section presents the results of electromagnetic simulations to study the radiation characteristics of the synthesized metasurfaces.

III. Full-wave analysis

The electromagnetic responses of each antenna were obtained by simulations in the K-band (18 GHz − 26 GHz) with 201 linearly spaced frequency samples. The main goal is to evaluate the electromagnetic characteristics of each metasurface, including metrics of field diversity required for computational imaging and localization applications. The reflection coefficients $|S_{11}|$ of each design are shown in Fig. 3.

The average values of the $|S_{11}|$ reflection coefficients are similar to all designs and remain around -10 dB, revealing that the input waves are effectively injected into the metasurfaces despite their resonant nature. Matching is influenced by the circular structure at the center of the antenna and the patterns generated by the reaction-diffusion model. The central patch, however, plays a crucial role, since signal transmission is primarily influenced by the initial interaction between the wave and the antenna. Consequently, the radius r is chosen to optimize antenna matching. In addition, the resonances highlighted by the dips in the frequency signal represent the various modes excited in the available band, which can be observed for all the antennas proposed. The electromagnetic performance related to each pattern based on the selected regions is evaluated by a quantitative analysis.

Firstly, the Q-factor is determined by the signal decay observed in the simulated time-domain reflection coefficient [9]. In Fig. 4, we present the Q-factor values for the proposed antennas. The irises (I) present the worst electromagnetic performances. The Q-factor can be improved by the reduction of the irises, in this turn, the radiation efficiency is depreciated. The designs (II) and (III) present the intermediary performances. Once the irises are added to the stripes design the Q-factor is depreciated and the radiation is improved, highlighting the trade-off between the Q-factor and radiation efficiency. In metasurface antenna design (IV), despite the similar characteristics of the simulated antennas, the dryland patterns present a slightly higher Q-factor, most likely due to the particular patch-shape-like design that favors the coupling among the elements and creates several coupled modes that contribute to increasing the Q-factor while keeping a reliable radiation efficiency.

The $Q-$factor and total radiation efficiency obtained for each metasurface are resumed in Table I. The dryland antenna gathers better electromagnetic characteristics for the considered computational DoA application, presenting a higher Q-factor ($Q = 214.25$), while maintaining a suitable radiation efficiency.

TABLE I: Comparison between different proposed antennas based on GS reaction-diffusion model.

Antenna design	Q-factor	Radiation efficiency (dB)
I	186.44	−7.76
II	204.78	−5.42
III	197.67	−4.52
IV	214.25	−5.81

The synthesis of these data reveals that structures II, III and IV exhibit very similar characteristics, despite the disparity in the type of patterns generated. This study thus seems to attest to a relatively universal form of average behavior for all these solutions. The assessment of metasurface antenna performance includes evaluating various metrics against specific requirements and constraints. As a result, this analysis is supplemented by spectral analysis using singular value decomposition (SVD), to determine the number of uncorrelated structures from a data set. In the proposed case, the decomposed matrix $\mathbf{H}$ corresponds to the set of radiation patterns calculated in the operating bandwidth (Fig. 5).

Despite the diversity of the patterns considered, these spectra reveal almost similar distributions of singular values. For each of these responses, an initial drop in the amplitude of the first singular values reflects the radiation of a field structure coherent in space and frequency dimensions [10]. This behavior may be attributed to the currents distributed uniformly on the central structure of each metasurface, assuming that the average impedance presented by the reaction-diffusion patterns is approximately equal. In each case, the spectra then tend to form a much shallower slope, a sign of great space-frequency diversity that can be exploited for computational imaging and localization applications. Based on the results, the dryland antenna presents the best performance. Therefore,

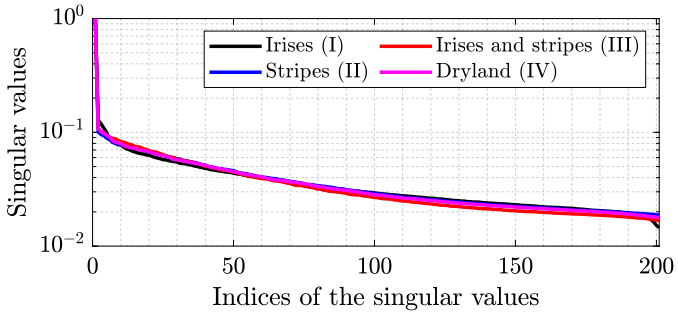

Fig. 5: Spectrum of singular values characterizing the space-frequency diversity of the fields radiated by each metasurface.

focusing now on the dryland morphogenetic metasurface and its optimized Q-factor, orthographic radiation patterns are extracted in the operating band and presented in Fig. 6.

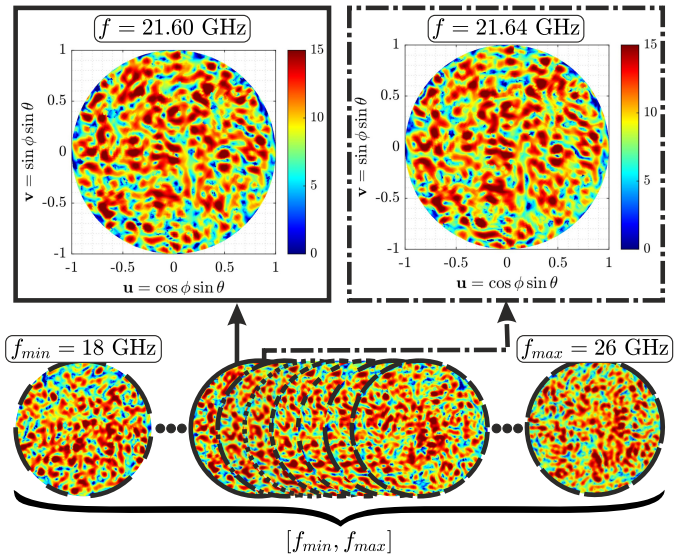

Fig. 6: Simulated electric-field radiation patterns within $[f_{min} = 18$ GHz, $f_{max} = 26$ GHz$]$ considering the dryland metasurface antenna.

In line with the Q-factors studied above, a simple 40 MHz variation yields weakly correlated far-field angle distributions (θ, ϕ). A more direct quantification of these dissimilarities is proposed by calculating the normalized frequency-frequency correlation matrix of the radiated fields (Fig. 6).

Moreover, the correlation coefficients among the radiation patterns across various frequencies are shown in Fig. 7. The diagonal shape of this correlation matrix ensures that spatial radiated field distributions are sufficiently dissimilar to ensure efficient conversion of spatial scene information into frequency signals measured on the antenna's coaxial port. These results thus confirm the capacity of dryland metasurface antenna to radiate uncorrelated fields when sweeping the operating frequency band, making it a good candidate for computational DoA applications.

IV. Direction of Arrival Estimation

A. Compressive framework

The aim of the computational DoA technique under consideration is to reconstruct the position of far-field sources from frequency measurements on a single port. Following on from previous demonstrations [1], a vector $\boldsymbol{\rho}$ corresponding to the position of the far-field sources is thus converted into a frequency signal $\mathbf{s}$ via the sensing matrix $\mathbf{H}$ constituted with the radiation patterns, leading to the relation $\mathbf{s} = \mathbf{H}\boldsymbol{\rho}$. The estimation of $\hat{\boldsymbol{\rho}}$ is finally carried out in this work by means of an iterative technique based on the generalized minimal residual (GMRES).

B. DoA evaluation

To assess the effectiveness of the dryland metasurface antenna for DoA applications the scheme proposed in Fig. 8 is simulated.

Fig. 8 shows a scheme for DoA evaluation considering the simulated far-field signals. Different sources of vertically polarized radiate toward the metasurface antenna considering the $[f_{min}, f_{max}]$ bandwidth. The dotted white lines in Fig. 9 represent the source's actual positions.

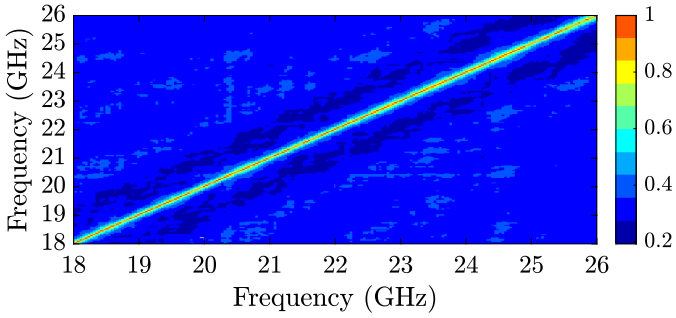

Fig. 7: Correlation coefficients of the radiation patterns of the dryland metasurface antenna.

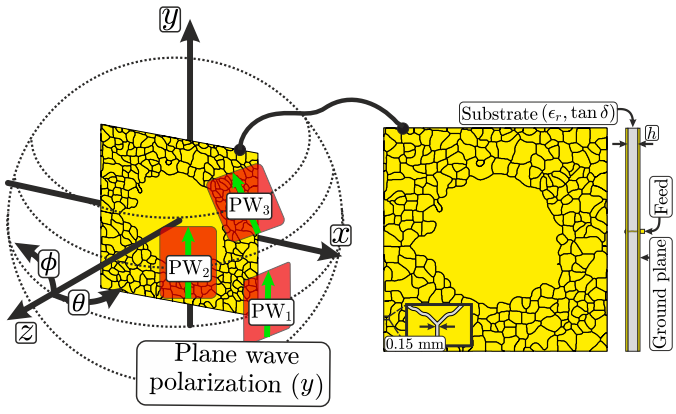

Fig. 8: Geometric parameters associated with the simulation of a computational DoA application. The morphogenetic metasurface antenna is positioned at the center of the coordinate system and illuminated by multiple sources located at PW$_1(\theta = 70°, \phi = 0°)$, PW$_2(\theta = 40°, \phi = 40°)$ and PW$_3(\theta = 50°, \phi = 20°)$.

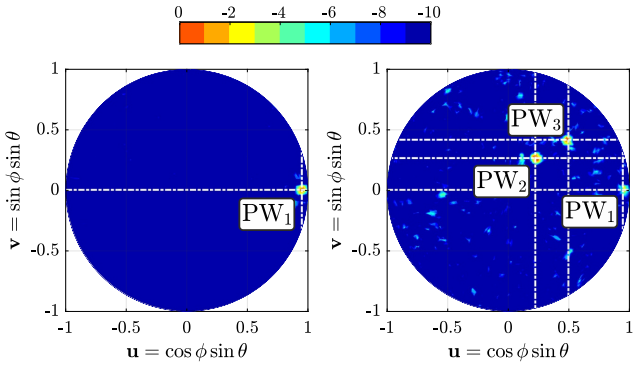

(a) (b)

Fig. 9: Normalized DoA estimation level ($\hat{\boldsymbol{\rho}}$) patterns when (a) a single source is present in the scene and when (b) three simultaneous sources are present in the scene.

Firstly, the metasurface antenna is illuminated by a single source at $\mathrm{PW}_1(\theta = 70°, \phi = 0°)$. The evaluated $\hat{\boldsymbol{\rho}}$ estimator is shown in Fig. 9(a). The spot indicates the evaluated localization and confirms the actual source position of the received signal. In Fig. 9(a), the source position is successfully retrieved.

A scenario where multiple sources are present is simulated, considering multiple planes waves of coordinates $\mathrm{PW}_1(\theta = 70°, \phi = 0°)$, $\mathrm{PW}_2(\theta = 40°, \phi = 40°)$ and $\mathrm{PW}_3(\theta = 50°, \phi = 20°)$. The evaluated $\hat{\boldsymbol{\rho}}$ estimator is shown in Fig. 9(b). The actual positions considering the signals $\mathrm{PW}_1, \mathrm{PW}_2$ are retrieved as shown in Fig. 9(b). However, angles greater than 70° lead to a low SNR received signal, making it more challenging to separate from other incoming signals. The received signal level decreases, since it approaches angles close to 70° as shown in Fig. 9(b). Then, the sensitivity for PW_3 is lower compared to other analyzed signals that impinge the metasurface antenna close to the antenna's main axis. Note, that a larger bandwidth $[f_{min}, f_{max}]$ can improve the distinction of incoming signals off-boresight direction since more available modes improve the distinctiveness capacity from low spatial sampled zones.

V. Conclusion

A morphogenetic metasurface generation technique has been introduced and evaluated for the design of frequency-diverse antennas applied to computational direction-of-arrival applications. This simple reaction-diffusion model generates metasurfaces compatible with simple manufacturing methods (photolithography, heat transfer, PCB milling). Four types of reaction-diffusion patterns have been investigated, enabling very similar characteristics to be achieved for the targeted applications, despite the diversity of shapes generated. Dryland structures were chosen for their interesting characteristics in terms of quality factor, linked to the frequency diversity used to encode the spatial information of the scenes to be reconstructed. This solution simplifies the data acquisition process by the compressive framework using a single measurement port, which can improve acquisition speed and relax the hardware constraints required for DoA applications. DoA is evaluated by taking into account a scenario in which one or more sources are present. The source's actual positions are successfully retrieved. The signal-to-noise ratio decreases as the angle of arrival of the signal moves away from the antenna axis. In situations where angles of arrival exceed $(\theta = 70°)$, it can be difficult to distinguish an incoming signal from background noise. The next steps are to produce and measure the metasurface antenna in a multipath environment.

VI. Acknowledgment

The authors acknowledge the support of the ANR JCJC MetaMorph (ANR-21-CE42-0005) and the Région Nouvelle-Aquitaine as part of the GPMR project.

References

[1] O. Yurduseven, M. A. B. Abbasi, T. Fromenteze, and V. Fusco, "Frequency-Diverse Computational Direction of Arrival Estimation Technique," *Scientific Reports*, vol. 9, no. 1, p. 16704, Nov. 2019. [Online]. Available: https://www.nature.com/articles/s41598-019-53363-3

[2] T. Fromenteze, O. Yurduseven, M. F. Imani, J. Gollub, C. Decroze, D. Carsenat, and D. R. Smith, "Computational imaging using a mode-mixing cavity at microwave frequencies," *Applied Physics Letters*, vol. 106, no. 19, p. 194104, May 2015. [Online]. Available: https://doi.org/10.1063/1.4921081

[3] M. F. Imani, T. Sleasman, J. N. Gollub, and D. R. Smith, "Analytical modeling of printed metasurface cavities for computational imaging," *Journal of Applied Physics*, vol. 120, no. 14, p. 144903, Oct. 2016. [Online]. Available: https://doi.org/10.1063/1.4964336

[4] O. Yurduseven, J. N. Gollub, T. Fromenteze, D. L. Marks, and D. R. Smith, "Optimization of frequency-diverse antennas for computational imaging at microwave frequencies," in *2017 11th European Conference on Antennas and Propagation (EUCAP)*, Mar. 2017, pp. 1410–1414.

[5] O. Yurduseven, V. R. Gowda, J. N. Gollub, and D. R. Smith, "Printed Aperiodic Cavity for Computational and Microwave Imaging," *IEEE Microwave and Wireless Components Letters*, vol. 26, no. 5, pp. 367–369, May 2016.

[6] ——, "Multistatic microwave imaging with arrays of planar cavities," *IET Microwaves, Antennas & Propagation*, vol. 10, no. 11, pp. 1174–1181, 2016, _eprint: https://onlinelibrary.wiley.com/doi/pdf/10.1049/iet-map.2015.0836. [Online]. Available: https://onlinelibrary.wiley.com/doi/abs/10.1049/iet-map.2015.0836

[7] P. Gray and S. K. Scott, "Autocatalytic reactions in the isothermal, continuous stirred tank reactor: Isolas and other forms of multistability," *Chemical Engineering Science*, vol. 38, no. 1, pp. 29–43, Jan. 1983. [Online]. Available: https://www.sciencedirect.com/science/article/pii/0009250983801328

[8] A. M. Turing, "The chemical basis of morphogenesis," *Philosophical Transactions of the Royal Society (part B)*, vol. 237, pp. 37–72, 1953.

[9] D. L. Marks, J. Gollub, and D. R. Smith, "Spatially resolving antenna arrays using frequency diversity," *JOSA A*, vol. 33, no. 5, pp. 899–912, 2016.

[10] T. Fromenteze, M. Davy, O. Yurduseven, Y. Marie-Joseph, and C. Decroze, "Spatiotemporal analysis of electromagnetic field coherence in complex media," *Physical Review Applied*, vol. 17, no. 5, p. 054039, 2022.